

Theoretical study of the effective modulus of a composite
considering the orientation distribution of the fillers and the
interfacial damage

Sangryun Lee¹ and Seunghwa Ryu^{1,*}

Affiliations

¹ Department of Mechanical Engineering, Korea Advanced Institute of Science and
Technology (KAIST), 291 Daehak-ro, Yuseong-gu, Daejeon 34141, Republic of Korea

* Corresponding author e-mail: ryush@kaist.ac.kr

Keywords

Homogenization, Micromechanics, Orientation average, Interfacial damage

Abstract

In the manufacturing process of a filler-reinforced composite, the fillers are partially aligned due to the shear flow in the drawing stage. Besides, various imperfections form at the interface between the matrix and the fillers, leading to debonding and slip under mechanical loading. There have been numerous micromechanics studies to predict effective moduli of the composites in the presence of partial alignment of fillers and interface imperfections. Here, we present an improved theory that overcomes two limitations in the existing micromechanics based approaches. First, we find that the interface damage tensor for axisymmetric ellipsoidal inhomogeneity developed to model the interfacial damage leads to the prediction of infinite or negative effective moduli. We show that these anomalies can be eliminated if correctly derived damage tensor is used. Second, we reveal that the previous theory on the effective moduli with axisymmetric filler orientation distribution fails because longitudinal and transverse moduli predictions do not converge in the limit of random orientation distribution. With appropriate corrections, we derive analytic expressions for the orientation average of arbitrary transversely isotropic 4th order tensor under general axisymmetric orientation distribution. We apply the improved method to compute the effective moduli of a polymer-carbon nanotube composite with non-uniform filler orientation and interface damage.

1. Introduction

Due to remarkable mechanical, electrical, and thermal properties, nanocomposites reinforced with carbon nanotubes (CNTs), graphene, and nanowires have attracted considerable attention because of their numerous potential applications, including flexible sensors (Amjadi et al., 2014; Lee et al., 2015), lithium batteries (Cui et al., 2008; Huang et al., 2002; Oh et al., 2010), optical device (Lü et al., 2006; Lü et al., 2005), and flexible energy storage devices (Nyholm et al., 2011; Pushparaj et al., 2007). To effectively design and make use of the nanocomposites, it is essential to accurately predict the effective properties of the composite as a function of shape, volume fraction, and orientation distribution of fillers.

For example, the piezoresistivity of the metal nanowire-polydimethylsiloxane (PDMS) composites has been utilized for the highly stretchable strain sensors (Amjadi et al., 2014). The effective electrical property of such composites has been analyzed by solving three dimensional electric circuit constructed from a percolation network of thousands of nanowires (Lee et al., 2015). For other examples, the finite element method (FEM) was used to compute the effective moduli of composites at the bulk scale (Banerjee and Sankar, 2014; Sodhani and Reese, 2014; Sun et al., 2001), whereas molecular dynamics (MD) simulations were used at the atomic scale (Alian et al., 2015; Yang et al., 2013a; Yang et al., 2013b). The above examples require computationally expensive and time-consuming calculations to consider large simulation cells involving many fillers to serve as representative volume elements (RVEs).

To compute the effective properties more efficiently, various micromechanics-based approaches have been used, such as the Eshelby method, the Mori-Tanaka (MT) method, and the Self-Consistent (SC) method. Eshelby was the first to introduce the Eshelby tensor (S) and to solve the single inhomogeneity in the matrix by converting the problem into an equivalent eigenstrain problem (Eshelby, 1957). The S tensor, which is a 4th order tensor that depends on

the matrix properties and the shape of fillers, relates the eigenstrain of inclusion (ε^*) and the constrained strain of the inclusion (ε_0) ($\varepsilon_0 = S: \varepsilon^*$) at single inclusion problem. As extensions of the approach, the MT method and the SC method were devised; these methods are mean-field homogenization schemes to treat the multiple inhomogeneity problems (Hill, 1965; Qiu and Weng, 1990; Withers et al., 1989). The MT method is the most popular method because it provides more accurate predictions on the effective properties than the Eshelby method and has an explicit closed-form solution, whereas the SC method relies on implicit equations. However, the original MT method has two limitations: first, it does not account for the imperfections in the filler-matrix interface, such as debonding and slip; second, it is only applicable when all fillers in the matrix are aligned perfectly along one direction.

To take into account the reduced effective modulus from the interfacial damage, Qu et al. introduced the interface spring model, which assumes a virtual linear spring at the interface to allow for a displacement jump across the interface (Qu, 1993). The 4th order interfacial damage tensor (R tensor) (which is referred to as H tensor in Qu et al. (Qu, 1993)) was defined to represent the degree of damage as a function of the filler shape and the compliance of the interface springs. The modified Eshelby tensor is then obtained by using the R tensor, which eventually leads to the change in the effective modulus prediction. Barai et al. firstly derived the closed form of the R tensor for the prolate shape filler (Barai and Weng, 2011). Because the shape of most fillers (such as spherical nanoparticles or carbon nanotube) can be approximated as axisymmetric ellipsoids with varying aspect ratio, the approach has been used to predict the effective moduli of various composites (Pan et al., 2013; Shokrieh et al., 2016; Yang et al., 2013b). Although incorrectly derived R tensor leads to the infinite or negative effective moduli for some ranges of filler aspect ratio, those anomalies have never been recognized in the previous studies (Pan et al., 2013; Shokrieh et al., 2016; Yang et al., 2013b).

The fillers in the matrix are partially aligned because of the shear flow in the drawing stage (Fan and Advani, 2005; Fu et al., 2000; Pötschke et al., 2005). Hence, it is crucial to predict the effective modulus as a function of the filler orientation distribution (Buck et al., 2015). Odegard et al. suggested the orientation average of 4th order stiffness tensor using the 3 – 1 – 3 Euler angle and showed that the effective moduli become anisotropic when the fillers are partially or fully aligned (Odegard et al., 2003). However, we find that their prediction on the effective moduli with axisymmetric filler orientation distribution fails because the longitudinal and transverse moduli do not converge in the limit of random orientation distribution due to the geometrical constraint of the Euler angle scheme. Meantime, the orientation average scheme of Odegard et al. has been applied to the study of the effective moduli of composites with various types (Alian et al., 2015; Nguyen et al., 2013; Pan et al., 2016).

To date, researchers have applied the micromechanics to predict the effective moduli of composites for either random or fully aligned orientation distribution of fillers when accounting for the interfacial damage (Dinzart and Sabar, 2017; Kundalwal and Kumar, 2016; Pan et al., 2013). For the studies considering realistic partial alignment of fillers (Dunn et al., 1996; Jiang et al., 2007; Nguyen et al., 2013), the imperfect interfacial bonding has not been considered. In this work, we propose an improved micromechanics model by correcting the two problems regarding the interface damage and the orientation average, and provide an efficient way of computing the effective moduli of composites for general axisymmetric orientation distribution of fillers. We demonstrate that the singularities in effective modulus prediction can be removed when the corrected R tensor is used. We obtain the closed form of R tensor for both prolate and oblate shape fillers and validate our results against the numerical integration results. We also confirm that our expressions of R tensor satisfy two limiting cases,

i.e., aspect ratio of 1 and infinity, at which analytic forms are readily available (Qu, 1993). Instead of the 3 – 1 – 3 Euler angle, we use polar and azimuthal angles on the unit sphere to represent the filler orientation and derive algebraic expressions of orientation average for the general transversely isotropic 4th order tensor under axisymmetric filler orientation distribution. We confirm that the longitudinal and transverse elastic moduli obtained from the correct R tensor and orientation average scheme converge in the random orientation distribution limit. Our results can be widely used to describe composites that include particles and fillers at various aspect ratios.

2. Micromechanics

2.1 Interfacial damage modeling

We adopt Hill's notation to calculate the effective modulus of RVE which is depicted in Fig. 1. Walpole's scheme is used to perform the complex calculations of 4th order tensors, such as double inner product and inverse conveniently (Qiu and Weng, 1990). In what follows, the capital sized alphabets represent 4th order tensors, and the colons denote double inner product. The effective stiffness tensor of the composite in the original MT approach is expressed as below.

$$L_{eff} = (c_0 L_0 + c_1 L_1 : A) : (c_0 I + c_1 A)^{-1} \quad (1)$$

where L_0 and L_1 are the stiffness tensors of the matrix and filler, respectively. I is the symmetric identity tensor. c_0 and c_1 refer to the volume fraction of matrix and fillers, respectively; thus, $c_0 + c_1 = 1$. In MT method, the tensor A is the local strain concentration tensor which relates the volume averaged strains in matrix ($\bar{\varepsilon}_0$) and fillers ($\bar{\varepsilon}_1$) by the definition of $\bar{\varepsilon}_1 \equiv A : \bar{\varepsilon}_0$. The local strain concentration tensor is obtained from a single inhomogeneity problem by comparing strain within the inhomogeneity and external strain ($\varepsilon_1 = A : \varepsilon_{ext}$). We do not need volume average here because the strain within the inhomogeneity is uniform. After solving linear elasticity for the single inhomogeneity problem, the A tensor can be expressed in terms of Eshelby tensor (S) and stiffness tensor of each phases (L_0, L_1), as Eq.(2).

$$A = [I + S : L_0^{-1} : (L_1 - L_0)]^{-1} \quad (2)$$

The Eshelby tensor (S) for the prolate and oblate inclusions has been derived in the literature (Qiu and Weng, 1990), as summarized in the Appendix.

Because the original MT method is only applicable when the fillers are completely

aligned and have perfect bonding with the matrix, the modified Mori-Tanaka (mMT) approach must be employed to account for the imperfect bonding at the interface (slip or debonding). To model the interfacial damage, we consider the displacement jump across the interface by adopting the linear spring model (Qu, 1993) (see Fig.2),

$$\Delta u_i = \eta_{ij} \sigma_{jk} n_k, \quad \eta_{ij} = \alpha \delta_{ij} + (\beta - \alpha) n_i n_j \quad (3)$$

where the η_{ij} tensor refers to the compliance of the interface spring in the tangential (α) and normal (β) directions. The n_i represents outward direction unit normal vector at the inclusion surface. After solving single inclusion problem with the displacement jump, the modified Eshelby tensor (\tilde{S}) is given as follows (Qu and Cherkaoui, 2006),

$$\tilde{S} = S + S : R : L_0 : (I - S). \quad (4)$$

In this work, we limit our focus on the axisymmetric (prolate and oblate) ellipsoidal fillers with two semi-axial lengths of a_1 along the x_1 direction and a along the x_2 and x_3 directions. Due to the nonphysical overlapping arising from a nonzero β (Luding, 2008), the R tensor is typically expressed by considering only tangential spring compliance as

$$R_{ijkl} = \alpha (P_{ijkl} - Q_{ijkl}) \quad (5)$$

where

$$P_{ijkl} = \frac{3}{16\pi} \int_0^\pi \left[\int_0^{2\pi} (\delta_{ik} \hat{n}_j \hat{n}_k + \delta_{jk} \hat{n}_i \hat{n}_l + \delta_{il} \hat{n}_k \hat{n}_j + \delta_{jl} \hat{n}_k \hat{n}_i) n^{-1} d\chi \right] \sin\psi d\psi \quad (6)$$

and

$$Q_{ijkl} = \frac{3}{4\pi} \int_0^\pi \left[\int_0^{2\pi} \hat{n}_i \hat{n}_j \hat{n}_k \hat{n}_l n^{-3} d\chi \right] \sin\psi d\psi. \quad (7)$$

with $\hat{\mathbf{n}} = \left(\frac{\cos\psi}{a_1}, \frac{\sin\psi \cos\chi}{a}, \frac{\sin\psi \sin\chi}{a} \right)^T$, $n = \sqrt{\hat{n}_i \hat{n}_i} = \frac{1}{\rho a} \sqrt{\cos^2 \psi + \rho^2 \sin^2 \psi}$, and $\rho = \frac{a_1}{a}$.

ψ and χ are two parameters that represent the surface integral domain, i.e. the surface of the

ellipsoidal inclusion. The non-zero independent components of P and Q can be obtained from the integral given below:

$$P_{1111} = \frac{3}{2a} \left[\frac{\rho}{(\rho^2 - 1)^{3/2}} \sin^{-1} \frac{\sqrt{\rho^2 - 1}}{\rho} - \frac{1}{\rho(\rho^2 - 1)} \right],$$

$$P_{2222} = \frac{3}{4a} \left[\frac{\rho(\rho^2 - 2)}{(\rho^2 - 1)^{3/2}} \sin^{-1} \frac{\sqrt{\rho^2 - 1}}{\rho} + \frac{\rho}{(\rho^2 - 1)} \right]$$

$$Q_{1111} = \frac{3}{2a} \left[\frac{2\rho^2 + 1}{\rho(\rho^2 - 1)^2} - \frac{3\rho}{(\rho^2 - 1)^{5/2}} \sin^{-1} \frac{\sqrt{\rho^2 - 1}}{\rho} \right]$$

$$Q_{1122} = \frac{3}{4a} \left[\frac{\rho(\rho^2 + 2)}{(\rho^2 - 1)^{5/2}} \sin^{-1} \frac{\sqrt{\rho^2 - 1}}{\rho} - \frac{3\rho}{(\rho^2 - 1)^2} \right]$$

$$Q_{2222} = \frac{9}{16a} \left[\frac{\rho(2 + \rho^2)}{(\rho^2 - 1)^2} + \frac{\rho^3(\rho^2 - 4)}{(\rho^2 - 1)^{5/2}} \sin^{-1} \frac{\sqrt{\rho^2 - 1}}{\rho} \right]$$

for prolate shape fillers ($\rho > 1$), and

$$P_{1111} = \frac{3}{2a} \left[-\frac{\rho}{(1 - \rho^2)^{3/2}} \sinh^{-1} \frac{\sqrt{1 - \rho^2}}{\rho} + \frac{1}{\rho(1 - \rho^2)} \right], \quad (8)$$

$$P_{2222} = \frac{3}{4a} \left[\frac{\rho(2 - \rho^2)}{(1 - \rho^2)^{3/2}} \sinh^{-1} \frac{\sqrt{1 - \rho^2}}{\rho} - \frac{\rho}{(1 - \rho^2)} \right]$$

$$Q_{1111} = \frac{3}{2a} \left[\frac{2\rho^2 + 1}{\rho(1 - \rho^2)^2} - \frac{3\rho}{(1 - \rho^2)^{5/2}} \sinh^{-1} \frac{\sqrt{1 - \rho^2}}{\rho} \right]$$

$$Q_{1122} = \frac{3}{4a} \left[\frac{\rho(\rho^2 + 2)}{(1 - \rho^2)^{5/2}} \sinh^{-1} \frac{\sqrt{1 - \rho^2}}{\rho} - \frac{3\rho}{(1 - \rho^2)^2} \right]$$

$$Q_{2222} = \frac{9}{16a} \left[\frac{\rho(2 + \rho^2)}{(1 - \rho^2)^2} - \frac{\rho^3(4 - \rho^2)}{(1 - \rho^2)^{5/2}} \sinh^{-1} \frac{\sqrt{1 - \rho^2}}{\rho} \right]$$

for oblate shape fillers ($\rho < 1$) with

$$P_{1212} = \frac{1}{4}(P_{1111} + P_{2222}), \quad P_{2323} = \frac{1}{2}P_{2222}, \quad Q_{2233} = \frac{1}{3}Q_{2222}$$

Other components can be obtained by using the symmetry condition in the 2-3 plane as well as the minor and major symmetry of P and Q tensors. In the limit of zero spring compliance (i.e. $\alpha = 0$), the modified Eshelby tensor(S) becomes the original Eshelby tensor(\tilde{S}) because R becomes zero tensor. The effective moduli in the mMT scheme can be obtained by replacing the original Eshelby tensor(S) with the modified Eshelby tensor(\tilde{S}) (Qu, 1993),

$$L_{eff} = (c_0 L_0 + c_1 L_1 : \tilde{A}) : (c_0 I + c_1 \tilde{A} + c_1 R : L_1 : \tilde{A})^{-1} \quad (9)$$

where \tilde{A} is the modified local strain concentration tensor, $\tilde{A} = [I + \tilde{S} : L_0^{-1} : (L_1 - L_0)]^{-1}$.

We plot the five independent P and Q components as functions of the aspect ratio ρ in Fig.3. We confirm that the newly derived analytic expression of Q_{1122} matches with the numerical integration obtained by Gaussian quadrature. In addition, our expression matches with the readily available analytic expressions at two limiting cases of $\rho = 1$ and $\rho = \infty$ in Qu et al. (Qu, 1993). We present the validation of all other nonzero components in Fig.3. We find that there exists a mathematical error in Q_{1122} component and typographical errors in the Q_{1111} and Q_{2222} components in the previous study (Barai and Weng, 2011; Hashemi, 2016) and that these errors were applied to the several follow-up studies (Barai and Weng, 2011; Pan et al., 2013; Shokrieh et al., 2016; Yang et al., 2013b). The uncorrected Q_{1122} diverges as the aspect ratio goes to unity and is larger than the correct value in the entire range of ρ . Because the R tensor affects modified Eshelby tensor and effective modulus, the effective moduli based on non-corrected R tensor have singularities at some values of the aspect ratio.

2.2 Orientation average scheme

The derived mathematical expression on the effective modulus is only applicable for the composites with completely aligned fillers. However, in the realistic composites, fillers are

randomly oriented or partially aligned (Fu et al., 2000; Pötschke et al., 2005; Zaixia et al., 2006) as depicted in Fig. 4. Because the originally randomly oriented fillers in the liquid-state matrix are drawn along one axis (X_1) in most manufacturing processes and experiments, we limit our focus on the axisymmetric orientation distribution. Following the previous studies(Odegard et al., 2003), we define the orientation averaged Mori-Tanaka (oaMT) as Eq. (10).

$$L_{eff} = (c_0 L_0 + c_1 \langle L_1: \tilde{A} \rangle): (c_0 I + c_1 \langle \tilde{A} \rangle + c_1 \langle R: L_1: \tilde{A} \rangle)^{-1} \quad (10)$$

where the operator $\langle \rangle$ denotes the orientation average of each tensor. When the orientation distribution $\lambda(\theta)$ is function of θ only, i.e. for axis-symmetry distribution, the orientation average of an arbitrary 4th order tensor X can be defined as

$$\langle X \rangle_{ijkl} = \frac{\int_0^{\frac{\pi}{2}} \int_{-\pi}^{\pi} X'_{ijkl}(\phi, \theta) \lambda(\theta) \sin(\theta) d\phi d\theta}{\int_0^{\frac{\pi}{2}} \int_{-\pi}^{\pi} \lambda(\theta) \sin \theta d\phi d\theta} \quad (11)$$

where θ and ϕ are azimuthal and polar angle with respect to the global coordinate (see Fig.5). X' is the tensor transformed to global coordinate system. Following the coordinate transformation rule of 4th order tensor with rotation matrix \mathbf{c} , X'_{ijkl} can be expressed as Eq.(12).

$$X'_{ijkl} = c_{ip} c_{jq} c_{kr} c_{ls} X_{pqrs} \quad \mathbf{c} = \begin{bmatrix} \cos\theta & -\sin\theta & 0 \\ \sin\theta \cos\phi & \cos\theta \cos\phi & -\sin\phi \\ \sin\theta \sin\phi & \cos\theta \sin\phi & \cos\phi \end{bmatrix} \quad (12)$$

The axisymmetric orientation distribution function can be categorized into three types: 3D random, normal distribution, and aligned.

$$\begin{aligned} \lambda(\theta) = 1 & \quad : \text{3D random distribution} \\ \lambda(\theta) = \exp(-k\theta^2) & \quad : \text{normal distribution} \\ \lambda(\theta) = \delta(\theta) & \quad : \text{aligned distribution} \end{aligned} \quad (13)$$

As visualized in Fig.6, when k in the normal distribution goes to zero or infinite, the

distribution converges to random or fully aligned distributions, respectively. We note that previously used 3 – 1 – 3 Euler angle set cannot describe the axisymmetric distribution along the X_1 axis due to the geometrical constraint, while several studies have adopted the 3 – 1 – 3 Euler angle set to describe the composites with axisymmetric filler orientation distribution (Alian et al., 2015; Nguyen et al., 2013; Pan et al., 2016). When k goes to zero, i.e., for a random orientation distribution, the composite must behave as an isotropic material. However, as shown in Fig.7, the longitudinal and transverse Young's modulus from the previous study do not converge to the same value in the random orientation limit. In contrast, the oaMT with our orientation average scheme predicts that both longitudinal and transverse moduli approach the modulus of the composite with randomly oriented fillers, whose analytic expression is available.

The evaluation of the orientation average in Eq. (11) is rather difficult because it involves complex transformations of 4th order tensor to global axis. Hence, no analytic expression exists on the orientation average for general axisymmetric distribution, whereas analytic expressions were derived for the two limiting cases of the 3D random and fully aligned distributions. To facilitate the use of the oaMT, we derive algebraic expressions of the orientation averaged transversely isotropic 4th order tensor under general axis-symmetry distribution of $\lambda(\theta)$. We express the orientation average of the transversely isotropic 4th order tensor $\langle A \rangle$ under arbitrary axis-symmetry distribution function, $\lambda(\theta)$, following Hill's notation, as

$$A = (2k_0, l_0, l'_0, n_0, 2m_0, 2p_0) \rightarrow \langle A \rangle = (2k_1, l_1, l'_1, n_1, 2m_1, 2p_1). \quad (14)$$

For the transversely isotropic 4th order material stiffness tensor, one can write Hooke's law using the six elastic constants, as follows,

$$\begin{aligned}
(\sigma_{22} + \sigma_{33}) &= 2k_0(\varepsilon_{22} + \varepsilon_{33}) + 2l'_0\varepsilon_{11}, \\
\sigma_{11} &= l_0(\varepsilon_{22} + \varepsilon_{33}) + n_0\varepsilon_{11}, \\
(\sigma_{22} - \sigma_{33}) &= 2n_0(\varepsilon_{22} - \varepsilon_{33}), \\
\sigma_{23} &= 2m_0\varepsilon_{23}, \quad \sigma_{12} = 2p_0\varepsilon_{12}, \quad \sigma_{13} = 2p_0\varepsilon_{13}
\end{aligned} \tag{15}$$

We find that the six independent components of $\langle A \rangle$ can be expressed as arithmetic sum of eight constants b_0, \dots, b_7 which are simple integrals including $\lambda(\theta)$.

$$\begin{aligned}
k_1 &= \frac{1}{4b_0} \left[k_0(b_0 + b_1 + 2b_2) + l_0(b_3 + b_4) + l'_0(b_3 + b_4) + m_0(b_0 + b_1 - 2b_2) + n_0(b_5) + p_0(4b_3) \right] \\
l_1 &= \frac{1}{2b_0} \left[k_0(b_3 + b_4) + l_0(b_1 + b_2) + l'_0(b_5) + n_0(b_3) + m_0(b_3 - b_4) + p_0(-4b_3) \right] \\
l'_1 &= \frac{1}{2b_0} \left[k_0(b_3 + b_4) + l(b_5) + l'_0(b_1 + b_2) + n_0(b_3) + m_0(b_3 - b_4) + p_0(-4b_3) \right] \\
n_1 &= \frac{1}{b_0} \left[k_0(b_5) + l_0(b_3) + l'_0(b_3) + n_0(b_1) + m_0(b_5) + p_0(4b_3) \right] \\
m_1 &= \frac{1}{8b_0} \left[k_0(b_0 + b_1 - 2b_2) + l_0(b_3 - b_4) + l'_0(b_3 - b_4) + n_0(b_5) + m_0(b_0 + b_1 + 6b_2) + p_0(4b_3 + 4b_4) \right] \\
p_1 &= \frac{1}{16b_0} \left[k_0(b_0 - b_7) + l_0(-b_0 + b_7) + l'_0(-b_0 + b_7) + n_0(b_0 - b_7) + m_0(5b_0 - 4b_6) + p_0(8b_0 + 4b_6 + 4b_7) \right]
\end{aligned} \tag{16}$$

where

$$\begin{aligned}
b_0 &= \int_0^{\frac{\pi}{2}} \lambda(\theta) \sin\theta d\theta & b_1 &= \int_0^{\frac{\pi}{2}} \lambda(\theta) \cos^4\theta \sin\theta d\theta & b_2 &= \int_0^{\frac{\pi}{2}} \lambda(\theta) \cos^2\theta \sin\theta d\theta \\
b_3 &= \int_0^{\frac{\pi}{2}} \lambda(\theta) \cos^2\theta \sin^3\theta d\theta & b_4 &= \int_0^{\frac{\pi}{2}} \lambda(\theta) \sin^3\theta d\theta & b_5 &= \int_0^{\frac{\pi}{2}} \lambda(\theta) \sin^5\theta d\theta \\
b_6 &= \int_0^{\frac{\pi}{2}} \lambda(\theta) \cos 2\theta d\theta & b_7 &= \int_0^{\frac{\pi}{2}} \lambda(\theta) \cos 4\theta d\theta
\end{aligned} \tag{17}$$

When $\lambda(\theta)$ is constant (3D random distribution function), the orientation average expression reproduces the analytic results of the random orientation case (Barai and Weng, 2011; Qiu and Weng, 1990; Yang et al., 2013b). We expect that our algebraic expression of orientation average can be widely applicable to the problems described by transversely isotropic 4th order tensors.

3. Results and Discussions

Table 1 Elastic constants used in the calculation of the effective moduli of the CNT-reinforced LaRC-CP2 polymer composite. The data are based on other research studies (Barai and Weng, 2011; Odegard et al., 2003), and the tangential compliance at interfacial damage between the polymer and CNT is set 10 nm/GPa (Barai and Weng, 2011).

Material properties	Matrix phase	Carbon nanotube (CNT)
Young's modulus (E)	0.85 GPa	
Poisson's ratio (ν)	0.4	
Longitudinal Young's modulus (E_{11})		1.06 TPa
Transverse bulk modulus (κ_{23})		271 GPa
Transverse shear modulus (μ_{23})		17 GPa
In-plane shear modulus (μ_{12})		442 GPa
In-plane Poisson's ratio (ν_{12})		0.162

We apply our oaMT with the interfacial damage correction to the prediction of the effective moduli of CNT-reinforced LaRC-CP2 polymers. The material constants used in our calculations are listed in Table 1. Following previous studies (Barai and Weng, 2011), we only consider the tangential part in the linear spring model (see Fig.2) and set the normal compliance to zero ($\beta = 0$) because finite normal spring compliance may cause a nonphysical configuration such as the overlap of the filler and matrix volumes. To avoid such a problem, it is necessary to set the spring compliance to be a non-linear function of the displacement jump, which makes the evaluation of effective moduli highly difficult (Wang et al., 2005), which is beyond the scope of this study. The tangential spring model can describe the interfacial slip.

3.1 Effective modulus of composite in the presence of interfacial damage

First, we compare the effective moduli of composites with the previous R tensor and the corrected R tensor. We correct two simple typographical errors in the Q_{1111} and Q_{2222} components, but leave the mathematical error in the Q_{1122} component when considering the previous R tensor. Fig.8 and Fig.9 depicts the elastic moduli as functions of the filler aspect ratio for the two limiting cases of fully random and fully aligned distributions respectively. Figs.8 show the Young's modulus and the shear modulus of the composite when the fillers are randomly oriented. Under perfect interfacial bonding condition, both elastic moduli increase with the aspect ratio of fillers at a given volume fraction (Fig.8). The moduli dramatically rise when the aspect ratio reaches approximately 100 and saturate when the aspect ratio exceed 1000. The same trend can be found in the longitudinal and transverse Young's modulus when fillers are fully aligned (Fig.9). We note that, when the interfacial imperfection is taken into account, the effective moduli should become lower than the perfect bonding condition. As shown in the Fig.8 and Fig.9, the effective moduli obtained from the previous R tensor are lower than those with perfect bonding in the most range. However, they have singularities near some aspect ratio values due to the presence of a singularity in the wrongly obtained Q_{1122} component. The singularity in the effective moduli can only be found when the aspect ratio is less than 100, and the number of singularities change with material properties of each phases and the volume fraction of fillers. The insets in Fig.8 and Fig.9 show that effective modulus at the aspect ratio of unity, i.e., $\rho = 1$. The effective moduli based on previous R tensor does not converge to the effective moduli of composite with spherical fillers, i.e., $\rho = 1$ (Qu, 1993). In comparison, the effective moduli obtained from the corrected R tensor are continuous functions of the aspect ratio, are always lower than their counterparts with perfect bonding condition, and converge to the known values for spherical fillers. We suspect that these

problems have not been identified because previous studies consider the composites having fillers in the range of very high aspect ratio ($> 1,000$) where the previous R tensor does not show a singularity (Barai and Weng, 2011; Pan et al., 2013; Shokrieh et al., 2016; Yang et al., 2013b). In addition, for large aspect ratio, the difference between the results with previous and corrected R tensors becomes rather negligible because the Q_{1122} component becomes nearly zero in the limit of large aspect ratio (Fig.3). However, we note that the use of the corrected R tensor is crucial in the small aspect ratio range smaller than 100.

3.2 Effective modulus of composite with partially aligned fillers

Second, we compute the effective modulus when the fillers are partially aligned with the orientation distribution of $\lambda(\theta) = \exp(-k\theta^2)$. We can study the effect of alignment by tuning the parameter k . The orientation averaged transversely isotropic tensor in Eq. (6) can be easily evaluated from the linear combinations of eight constants. Figs.10 show the change of longitudinal and transverse Young's modulus with k and aspect ratio ρ at a fixed volume fraction (2.5%). Because the moduli are calculated from the corrected R tensor, they do not suffer from singularity problems. When the degree of filler alignment reduces (i.e., when k decreases), the difference between two moduli diminishes and they eventually converges at $k = 0$. We find that both moduli increase with the aspect ratio. In contrast, when k increases, the longitudinal modulus increases whereas the transverse modulus decreases, as expected. We also demonstrate the combined effect of volume fraction and orientation distribution in Fig.11. Both moduli increase when the volume fraction increases, and they approach the modulus of matrix in the zero volume fraction limit. We note that the contour plot depicted in Fig.11 can be easily obtained for any arbitrary axisymmetric orientation distribution of axisymmetric ellipsoidal fillers by computing the eight constants b_0, \dots, b_7 . which will facilitate the use of

the micromechanics approach in designing and predicting the performance of the composites.

4. Conclusions

We computed the effective moduli of composites as functions of the aspect ratio of fillers, degree of orientation in the presence of interfacial damage. With appropriate corrections in the interfacial damage tensor and orientation average scheme, the spurious singularities in the effective composite modulus predictions are eliminated, and the longitudinal and transverse moduli converges in the limit of random orientation distribution of fillers. We demonstrated that the magnitude of moduli can be tuned by either the aspect ratio or the volume fraction, and that the directional elastic properties can be tuned by controlling the orientation distribution of fillers. To facilitate the application of our method, we derived an analytic expression for the orientation average for arbitrary axisymmetric filler orientation distribution. We believe that our study can provide a comprehensive guidance in the effort to tune the effective moduli of composite materials.

Acknowledgments

The authors acknowledge the support of the Basic Science Research Program through the National Research Foundation of Korea (NRF) funded by the Ministry of Science, ICT & Future Planning (2016R1C1B2011979) and the support from the Agency for Defense Development of Korea (15-201-701-008).

Figure Set

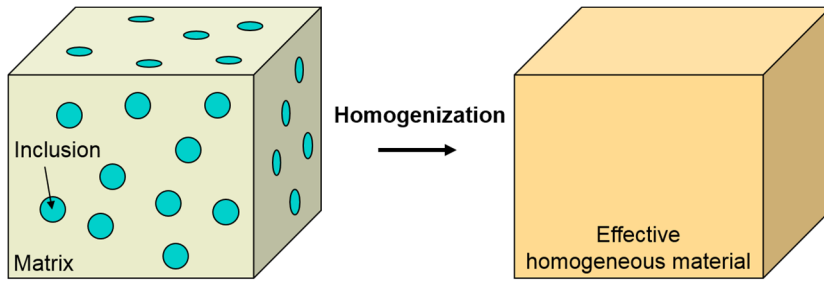


Fig.1 Schematic of homogenization scheme for RVE of reinforced composite.

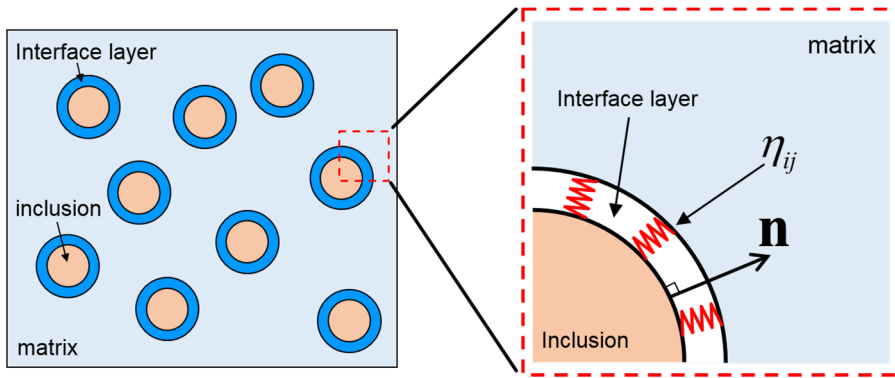


Fig.2 Interface spring model to simulate the damaged interface between matrix and filler. To visualize the interface spring, we draw a gap at the interface whose thickness is originally zero.

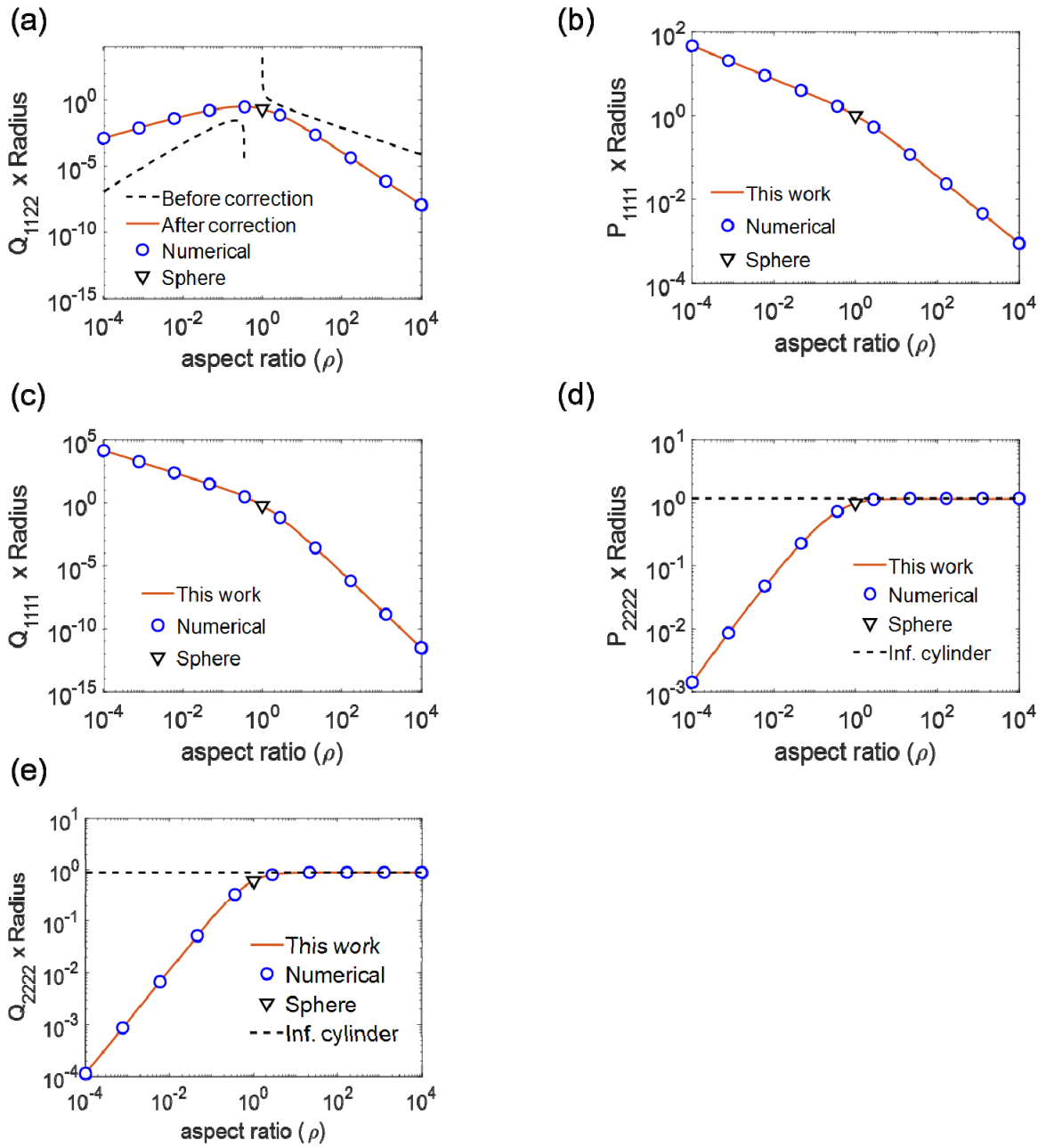


Fig.3 Independent components in P and Q tensor respect to aspect ratio of the filler. Previous and corrected Q_{1122} component, one of the damaged interface properties components, with respect to the aspect ratio of the filler. The triangular symbol and dashed line are the known value at the aspect ratio of 1 and infinite respectively, reported by (Qu, 1993).

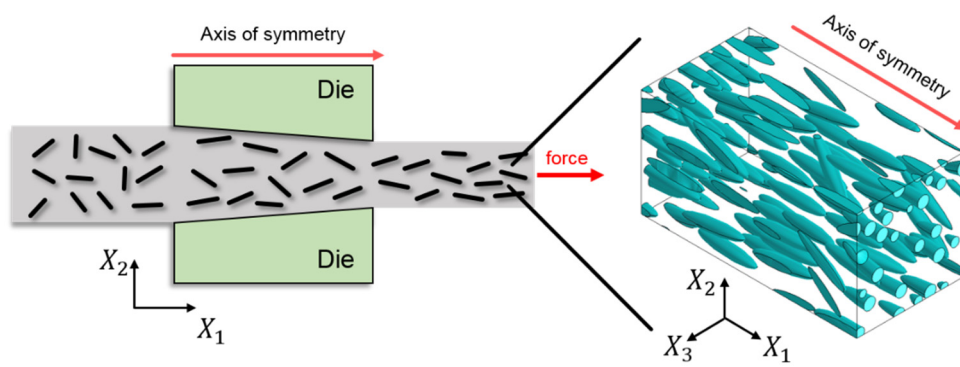


Fig.4 The drawing process at composite manufacturing process and the microstructure of composite after process.

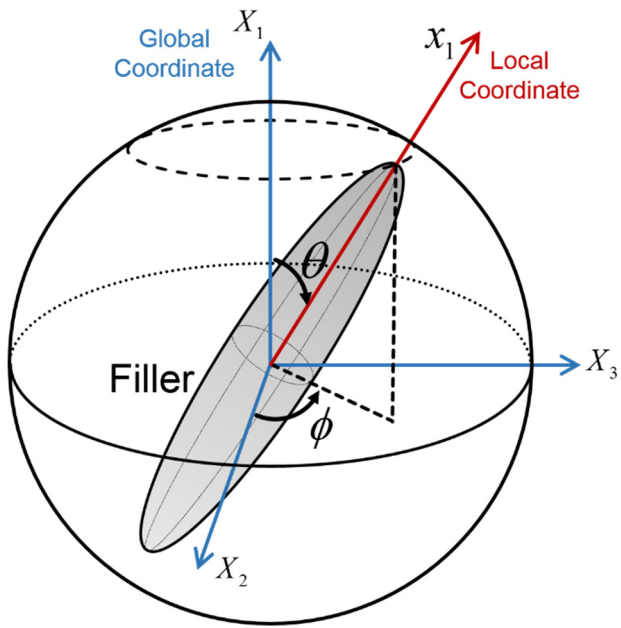


Fig.5 The local coordinates (x_1, x_2, x_3) and global coordinates (X_1, X_2, X_3) displayed with the spherical coordinates.

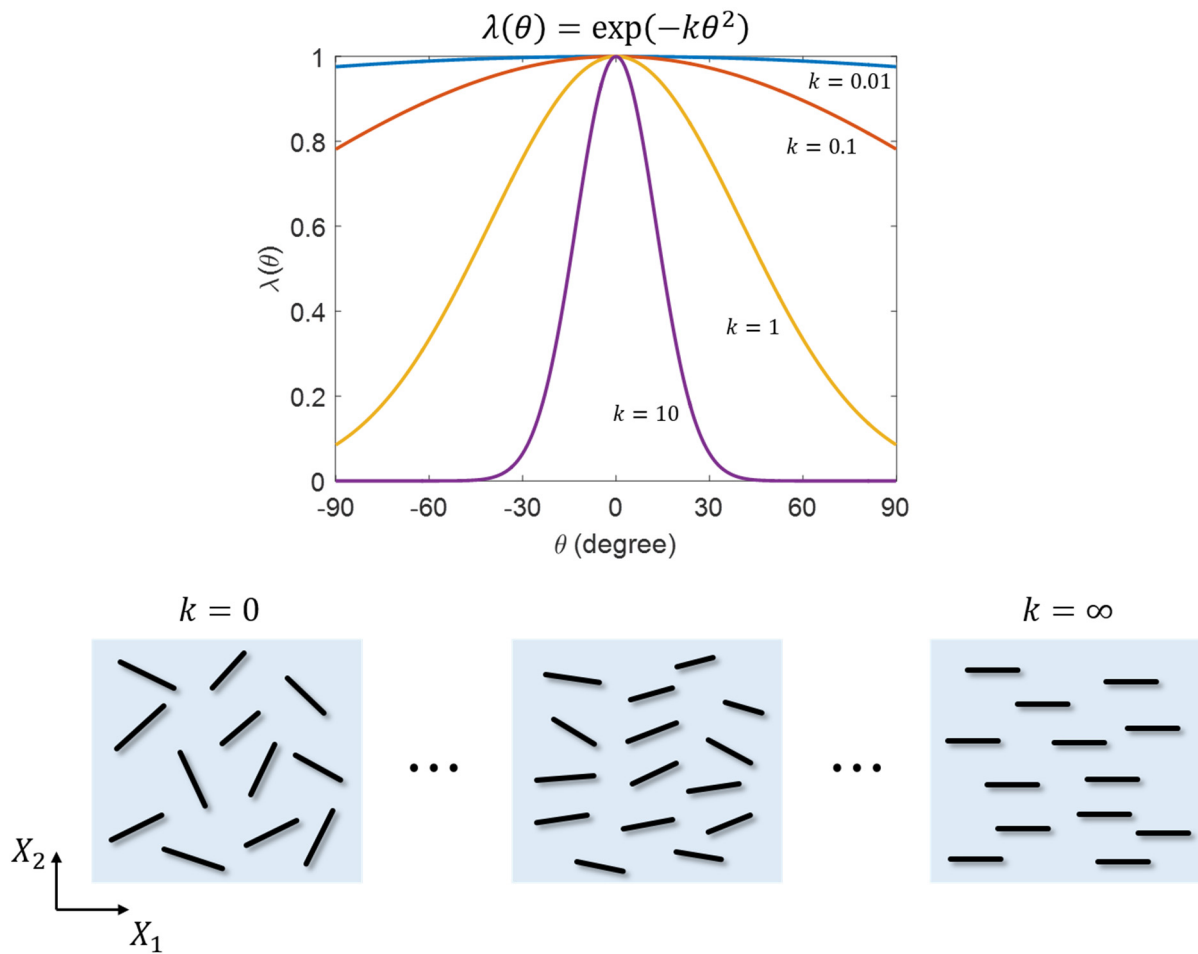


Fig.6 Various orientation distribution functions of fillers in composite respect to different k value and the microstructure for corresponding k value.

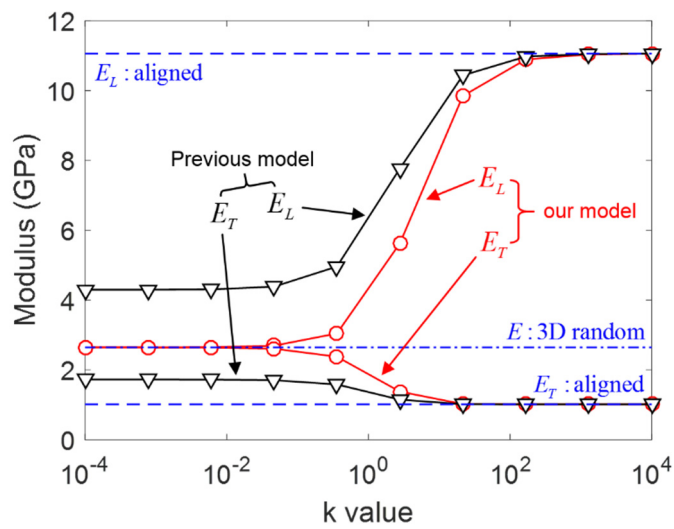


Fig.7 Modulus in the longitudinal (X_1) and transverse directions (X_2, X_3). The dashed lines are the results from known analytic expressions. The parameters used in calculation are listed in Table 1, and the volume concentration (c_1) is 1%.

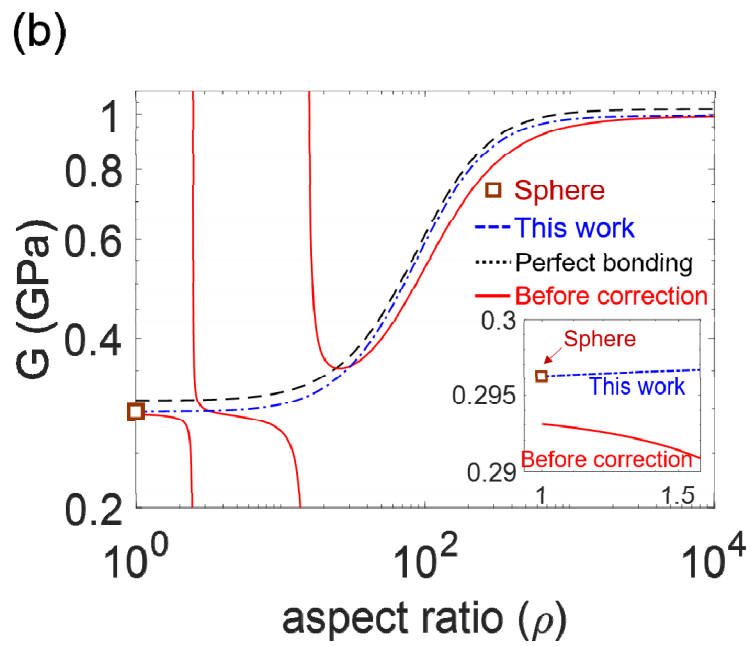
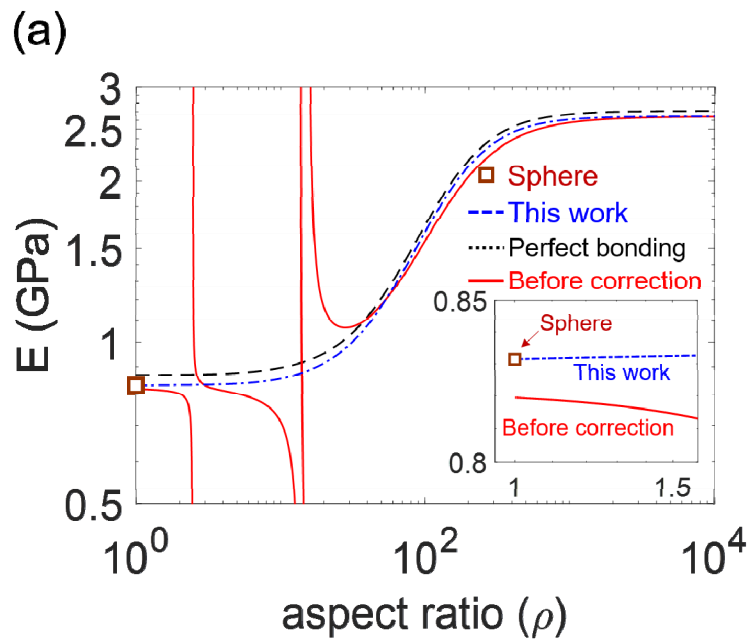
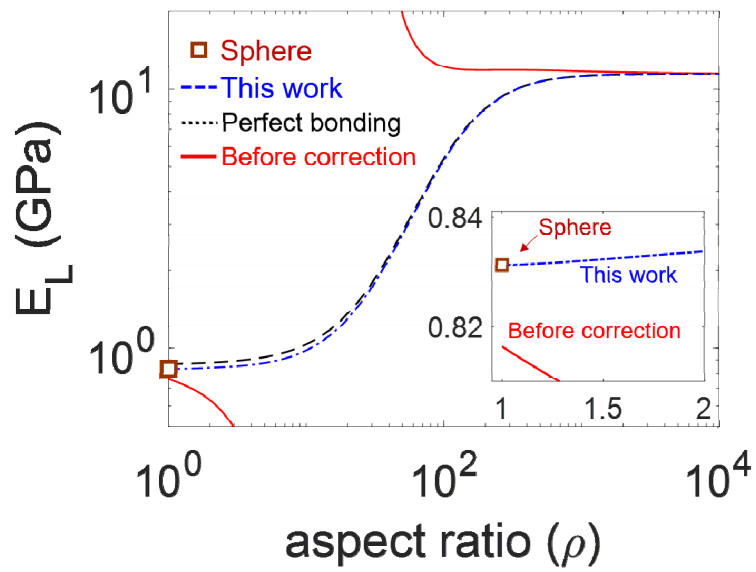


Fig.8 (a) Effective Young's modulus and (b) shear modulus of a composite with randomly oriented fillers with 1% volume concentration. The inset in each figure show the results near the aspect ratio of 1.

(a)



(b)

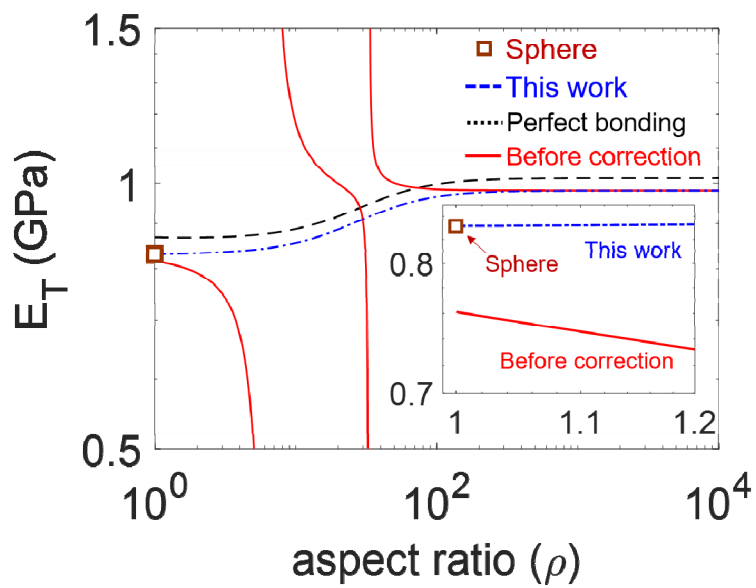


Fig.9 (a) Longitudinal Young's modulus and (b) transverse Young's modulus of a composite whose orientation distribution of fillers is aligned distribution. The volume concentration of fillers is 1%.

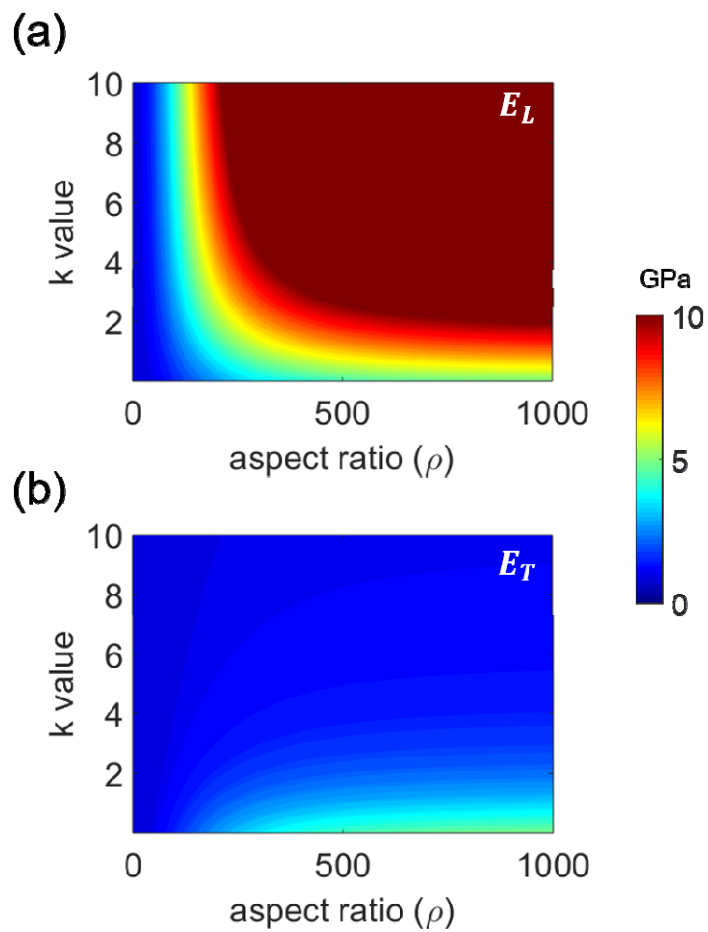


Fig.10 (a) Longitudinal Young's modulus(E_L) and (b) transverse Young's modulus(E_T) with a normal distribution of fillers as functions of k value and aspect ratio of fillers under fixed volume fraction (2.5%)

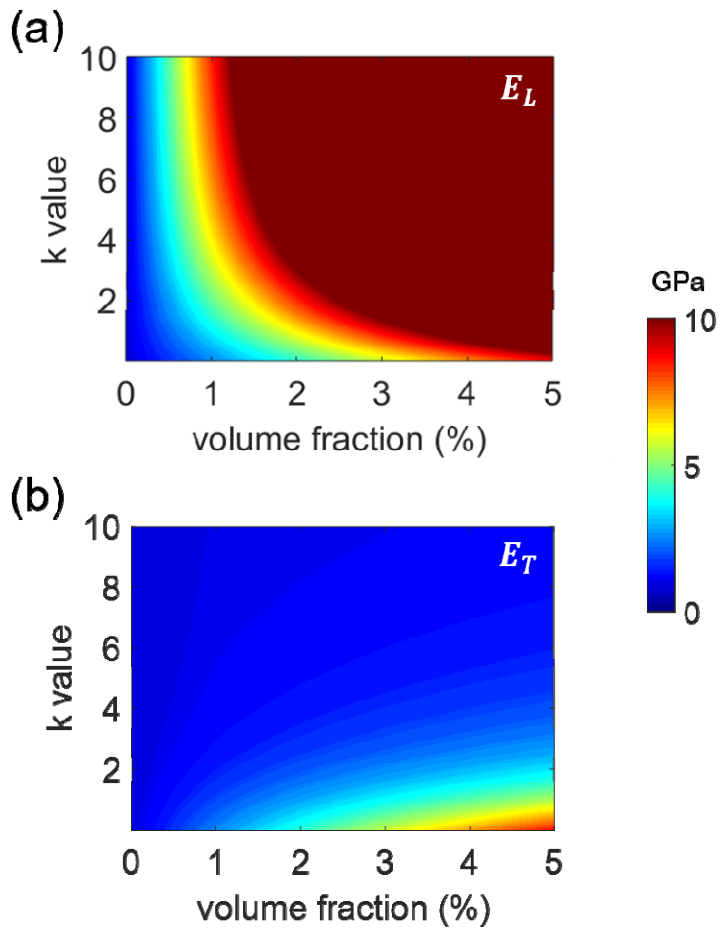


Fig.11 (a) Longitudinal(E_L) and (b) transverse(E_T) Young's modulus with respect to the degree of orientation (k) and the volume fraction of the fillers under fixed aspect ratio 1000.

Appendix: Eshelby tensor (S) for ellipsoidal shape inclusion.

For an ellipsoidal inclusion with symmetric axis(x1) in isotropic matrix, Eshelby tensor can be expressed as below,

$$S_{1111} = \frac{1}{2(1-\nu_0)} \left\{ 1 - 2\nu_0 + \frac{3\rho^2 - 1}{\rho^2 - 1} - \left[1 - 2\nu_0 + \frac{3\rho^2}{\rho^2 - 1} \right] g \right\}$$

$$S_{2222} = S_{3333} = \frac{3}{8(1-\nu_0)} \frac{\rho^2}{\rho^2 - 1} + \frac{1}{4(1-\nu_0)} \left[1 - 2\nu_0 - \frac{9}{4(\rho^2 - 1)} \right] g$$

$$S_{2233} = S_{3322} = \frac{1}{4(1-\nu_0)} \left\{ \frac{\rho^2}{2(\rho^2 - 1)} - \left[1 - 2\nu_0 + \frac{3}{4(\rho^2 - 1)} \right] g \right\}$$

$$S_{2211} = S_{3311} = -\frac{1}{2(1-\nu_0)} \frac{\rho^2}{\rho^2 - 1} + \frac{1}{4(1-\nu_0)} \left\{ \frac{3\rho^2}{\rho^2 - 1} - (1 - 2\nu_0) \right\} g$$

$$S_{1122} = S_{1133} = -\frac{1}{2(1-\nu_0)} \left[1 - 2\nu_0 + \frac{1}{\rho^2 - 1} \right] + \frac{1}{2(1-\nu_0)} \left[1 - 2\nu_0 + \frac{3}{2(\rho^2 - 1)} \right] g$$

$$S_{2323} = \frac{1}{4(1-\nu_0)} \left\{ \frac{\rho^2}{2(\rho^2 - 1)} + \left[1 - 2\nu_0 - \frac{3}{4(\rho^2 - 1)} \right] g \right\}$$

$$S_{1212} = S_{1313} = \frac{1}{4(1-\nu_0)} \left\{ 1 - 2\nu_0 - \frac{\rho^2 + 1}{\rho^2 - 1} - \frac{1}{2} \left[1 - 2\nu_0 - \frac{3(\rho^2 + 1)}{\rho^2 - 1} \right] g \right\}$$

Where ρ is the aspect ratio of filler and ν_0 is Poisson ratio of matrix. Other components can be obtained by using minor symmetry condition ($S_{ijkl} = S_{jikl} = S_{ijlk}$). The g is given by

$$g = \frac{\rho}{(\rho^2 - 1)^{3/2}} \left\{ \rho(\rho^2 - 1)^{\frac{1}{2}} - \cosh^{-1} \rho \right\} \quad \text{prolate shape}$$

$$= \frac{\rho}{(1 - \rho^2)^{3/2}} \left\{ \cos^{-1} \rho - \rho(1 - \rho^2)^{\frac{1}{2}} \right\} \quad \text{oblate shape}$$

References

- Alian, A.R., Kundalwal, S.I., Meguid, S.A., 2015. Interfacial and mechanical properties of epoxy nanocomposites using different multiscale modeling schemes. *Composite Structures* 131, 545-555.
- Amjadi, M., Pichitpajongkit, A., Lee, S., Ryu, S., Park, I., 2014. Highly Stretchable and Sensitive Strain Sensor Based on Silver Nanowire–Elastomer Nanocomposite. *ACS Nano* 8, 5154-5163.
- Banerjee, S., Sankar, B.V., 2014. Mechanical properties of hybrid composites using finite element method based micromechanics. *Composites Part B: Engineering* 58, 318-327.
- Barai, P., Weng, G.J., 2011. A theory of plasticity for carbon nanotube reinforced composites. *International Journal of Plasticity* 27, 539-559.
- Buck, F., Brylka, B., Müller, V., Müller, T., Weidenmann, K.A., Hrymak, A.N., Henning, F., Böhlke, T., 2015. Two-scale structural mechanical modeling of long fiber reinforced thermoplastics. *Composites Science and Technology* 117, 159-167.
- Cui, G., Gu, L., Zhi, L., Kaskhedikar, N., van Aken, P.A., Müllen, K., Maier, J., 2008. A Germanium–Carbon Nanocomposite Material for Lithium Batteries. *Advanced Materials* 20, 3079-3083.
- Dinzart, F., Sabar, H., 2017. New micromechanical modeling of the elastic behavior of composite materials with ellipsoidal reinforcements and imperfect interfaces. *International Journal of Solids and Structures* 108, 254-262.
- Dunn, M.L., Ledbetter, H., Heyliger, P.R., Choi, C.S., 1996. Elastic constants of textured short-fiber composites. *Journal of the Mechanics and Physics of Solids* 44, 1509-&.
- Eshelby, J.D., 1957. The Determination of the Elastic Field of an Ellipsoidal Inclusion, and Related Problems. *Proceedings of the Royal Society of London A: Mathematical, Physical and Engineering Sciences* 241, 376-396.
- Fan, Z., Advani, S.G., 2005. Characterization of orientation state of carbon nanotubes in shear flow. *Polymer* 46, 5232-5240.
- Fu, S.Y., Lauke, B., Mäder, E., Yue, C.Y., Hu, X., 2000. Tensile properties of short-glass-fiber- and short-carbon-fiber-reinforced polypropylene composites. *Composites Part A: Applied Science and Manufacturing* 31, 1117-1125.
- Hashemi, R., 2016. On the overall viscoelastic behavior of graphene/polymer nanocomposites with imperfect interface. *International Journal of Engineering Science* 105, 38-55.
- Hill, R., 1965. A self-consistent mechanics of composite materials. *Journal of the Mechanics and Physics of Solids* 13, 213-222.
- Huang, H., Yin, S.C., Kerr, T., Taylor, N., Nazar, L.F., 2002. Nanostructured Composites: A High Capacity, Fast Rate Li₃V₂(PO₄)₃/Carbon Cathode for Rechargeable Lithium Batteries. *Advanced Materials* 14, 1525-1528.
- Jiang, B., Liu, C., Zhang, C., Wang, B., Wang, Z., 2007. The effect of non-symmetric distribution of fiber orientation and aspect ratio on elastic properties of composites. *Compos Part B-Eng* 38, 24-34.
- Kundalwal, S.I., Kumar, S., 2016. Multiscale modeling of stress transfer in continuous microscale fiber

reinforced composites with nano-engineered interphase. *Mechanics of Materials* 102, 117-131.

Lee, S., Amjadi, M., Pugno, N., Park, I., Ryu, S., 2015. Computational analysis of metallic nanowire-elastomer nanocomposite based strain sensors. *AIP Advances* 5, 117233.

Lü, C., Cheng, Y., Liu, Y., Liu, F., Yang, B., 2006. A Facile Route to ZnS–Polymer Nanocomposite Optical Materials with High Nanophase Content via γ -Ray Irradiation Initiated Bulk Polymerization. *Advanced Materials* 18, 1188-1192.

Lü, C., Guan, C., Liu, Y., Cheng, Y., Yang, B., 2005. PbS/Polymer Nanocomposite Optical Materials with High Refractive Index. *Chemistry of Materials* 17, 2448-2454.

Luding, S., 2008. Cohesive, frictional powders: contact models for tension. *Granular Matter* 10, 235.

Nguyen, H.G., Ortola, S., Ghorbel, E., 2013. Micromechanical modelling of the elastic behaviour of polymer mortars. *European Journal of Environmental and Civil Engineering* 17, 65-83.

Nyholm, L., Nyström, G., Mihranyan, A., Strømme, M., 2011. Toward Flexible Polymer and Paper-Based Energy Storage Devices. *Advanced Materials* 23, 3751-3769.

Odegard, G.M., Gates, T.S., Wise, K.E., Park, C., Siochi, E.J., 2003. Constitutive modeling of nanotube-reinforced polymer composites. *Composites Science and Technology* 63, 1671-1687.

Oh, S.-M., Oh, S.-W., Yoon, C.-S., Scrosati, B., Amine, K., Sun, Y.-K., 2010. High-Performance Carbon-LiMnPO₄ Nanocomposite Cathode for Lithium Batteries. *Advanced Functional Materials* 20, 3260-3265.

Pan, J., Bian, L., Zhao, H., Zhao, Y., 2016. A new micromechanics model and effective elastic modulus of nanotube reinforced composites. *Computational Materials Science* 113, 21-26.

Pan, Y., Weng, G.J., Meguid, S.A., Bao, W.S., Zhu, Z.H., Hamouda, A.M.S., 2013. Interface effects on the viscoelastic characteristics of carbon nanotube polymer matrix composites. *Mechanics of Materials* 58, 1-11.

Pötschke, P., Brüinig, H., Janke, A., Fischer, D., Jehnichen, D., 2005. Orientation of multiwalled carbon nanotubes in composites with polycarbonate by melt spinning. *Polymer* 46, 10355-10363.

Pushparaj, V.L., Shaijumon, M.M., Kumar, A., Murugesan, S., Ci, L., Vajtai, R., Linhardt, R.J., Nalamasu, O., Ajayan, P.M., 2007. Flexible energy storage devices based on nanocomposite paper. *Proceedings of the National Academy of Sciences* 104, 13574-13577.

Qiu, Y.P., Weng, G.J., 1990. On the application of Mori-Tanaka's theory involving transversely isotropic spheroidal inclusions. *International Journal of Engineering Science* 28, 1121-1137.

Qu, J., 1993. The effect of slightly weakened interfaces on the overall elastic properties of composite materials. *Mechanics of Materials* 14, 269-281.

Qu, J., Cherkaoui, M., 2006. *Fundamentals of Micromechanics of Solids*. John Wiley & Sons, Inc.

Shokrieh, M.M., Ghajar, R., Shajari, A.R., 2016. The effect of time-dependent slightly weakened interface on the viscoelastic properties of CNT/polymer nanocomposites. *Composite Structures* 146, 122-131.

Sodhani, D., Reese, S., 2014. Finite Element-Based Micromechanical Modeling of Microstructure Morphology in Filler-Reinforced Elastomer. *Macromolecules* 47, 3161-3169.

Sun, H., Di, S., Zhang, N., Wu, C., 2001. Micromechanics of composite materials using multivariable

finite element method and homogenization theory. *International Journal of Solids and Structures* 38, 3007-3020.

Wang, J., Duan, H.L., Zhang, Z., Huang, Z.P., 2005. An anti-interpenetration model and connections between interphase and interface models in particle-reinforced composites. *International Journal of Mechanical Sciences* 47, 701-718.

Withers, P.J., Stobbs, W.M., Pedersen, O.B., 1989. The application of the eshelby method of internal stress determination to short fibre metal matrix composites. *Acta Metallurgica* 37, 3061-3084.

Yang, B.J., Shin, H., Lee, H.K., Kim, H., 2013a. A combined molecular dynamics/micromechanics/finite element approach for multiscale constitutive modeling of nanocomposites with interface effects. *Applied Physics Letters* 103, 241903.

Yang, S., Yu, S., Ryu, J., Cho, J.-M., Kyoung, W., Han, D.-S., Cho, M., 2013b. Nonlinear multiscale modeling approach to characterize elastoplastic behavior of CNT/polymer nanocomposites considering the interphase and interfacial imperfection. *International Journal of Plasticity* 41, 124-146.

Zaixia, F., Zhangyu, Yanmo, C., Hairu, L., 2006. Effects of Pre-stretching on the Tensile Properties of Knitted Glass Fiber Fabric Reinforced Polypropylene Composite. *Journal of Thermoplastic Composite Materials* 19, 399-411.